X-Ray Photoelectron Spectroscopy Investigations of Carbon-Coated Li_xFePO_4 Materials

R. Dedryvère,*,† M. Maccario,‡,§ L. Croguennec,‡,§ F. Le Cras,|| C. Delmas,‡,§ and D. Gonbeau†

IPREM/ECP (UMR 5254), Université de Pau, Hélioparc, 2 avenue Pierre Angot, 64053 Pau cedex 9, France, CNRS, Institut de Chimie de la Matière Condensée de Bordeaux, Pessac cedex F33608, France, Université de Bordeaux, Institut de Chimie de la Matière Condensée de Bordeaux, ENSCPB, Pessac cedex F33608, France, Commissariat à l'Énergie Atomique, Laboratoire Composants pour l'Énergie DRT/LITEN/DTNM/LCE, 17 rue des Martyrs, 38054 Grenoble cedex 9, France

Received July 22, 2008. Revised Manuscript Received September 28, 2008

Because of its surface sensitivity, X-ray photoelectron spectroscopy allowed us to access the mechanisms at the very surface of 100 nm diameter carbon-coated $LiFePO_4$ nanoparticles. A continuous evolution of the Fe^{3+}/Fe^{2+} ratio was observed at the surface of the particles upon charge and discharge, in good agreement with the change in the average lithium content of Li_xFePO_4 electrode material. These results support these models considering migration of a reaction front along the *a*-axis inside the cristallites vs. the shrinking-core model, to describe lithium (de)intercalation in $LiFePO_4$. XPS analyses showed also that electrode/electrolyte interface phenomena are minimized using carbon-coated $LiFePO_4$ particles as positive electrode material vs $LiCoO_2$ for instance, despite the nanometric size of the particles.

1. Introduction

$LiFePO_4$ was shown to be a very interesting candidate as positive electrode material for lithium-ion batteries[1] with, when synthesized in optimized conditions, a high reversible capacity (∼160 mA h/g at *C*/10) at an average voltage of ∼ 3.5 V vs Li^+/Li[2] and an excellent structural stability upon long time cycling[3,4] in the charged state.[5,6] A very important improvement was proposed by Ravet et al.;[7] thanks to the use of a carbonaceous precursor, they obtained nanoparticles with a carbon coating that increases the electronic conductivity of the material at the macroscopic scale.[7−15]

The lithium deintercalation/intercalation mechanism in "Li_xFePO_4" is commonly described as a two-phase reaction, in good agreement with the ∼3.5 V vs Li^+/Li plateau present on the cycling curve between a lithium-rich phase ($Li_{1-\epsilon}FePO_4$, $\varepsilon \rightarrow 0$) and a lithium-deficient phase ($Li_{\varepsilon'}FePO_4$, $\varepsilon' \rightarrow 0$).[1,16] Two solid-solution domains, more or less extended in compositions, are observed at the two ends of the electrochemical process.[17,18] The two-phase mechanism was first described by Padhi and co-workers considering a shrinking-core model, with the migration of an $FePO_4$/$LiFePO_4$ interface inward each particle and the formation upon charge of a lithium-deficient shell ($Li_{\varepsilon'}FePO_4$) from the surface leading to a continuous shrinking of the lithium-rich core ($Li_{1-\varepsilon}FePO_4$).[1] The reverse phenomenon would occur upon discharge. In fact, high-resolution transmission electron microscopy performed by Chen et al. [19] and more recently by Laffont et al.[20] clearly revealed the formation of $FePO_4$ and $LiFePO_4$ domains in platelet-like primary particles, in good agreement with a preferential lithium ions diffusion in the *b*-axis direction, as predicted by theoretical studies of

* Corresponding author. Tel.: (33) 5 59 40 75 97. E-mail: remi.dedryvere@univ-pau.fr.
† Université de Pau.
‡ CNRS, Institut de Chimie de la Matière Condensée de Bordeaux.
§ Université de Bordeaux, Institut de Chimie de la Matière Condensée de Bordeaux.
|| Commissariat à l'Énergie Atomique.

(1) Padhi, A. K.; Nanjundaswamy, K. S.; Goodenough, J. B. *J. Electrochem. Soc.* **1997**, *144*, 1188.
(2) Franger, S.; Bourbon, C.; Le Cras, F. *J. Electrochem. Soc.* **2004**, *151*, A1024–A1027.
(3) Amine, K.; Liu, J.; Belharouak, I. *Electrochem. Commun.* **2005**, *7*, 669–673.
(4) Liao, X. Z.; Ma, Z. F.; He, Y. S.; Zhang, X. M.; Wang, L.; Jiang, Y. *J. Electrochem. Soc.* **2005**, *152*, A1969–A1973.
(5) Delacourt, C.; Poizot, P.; Tarascon, J. M.; Masquelier, C. *Nat. Mater.* **2005**, *4*, 254–260.
(6) Dodd, J. L.; Yazami, R.; Fultz, B. *Electrochem. Solid-State Lett.* **2006**, *9*, A151–A155.
(7) Ravet, N.; Chouinard, Y.; Magnan, J. F.; Besner, S.; Gauthier, M.; Armand, M. *J. Power Sources* **2001**, *97−98*, 503–507.
(8) Yamada, A.; Chung, S. C.; Hinokuma, K. *J. Electrochem. Soc.* **2001**, *148*, A224.
(9) Franger, S.; Le Cras, F.; Bourbon, C.; Rouault, H. *J. Power Sources* **2003**, *119*, 252–257.
(10) Andersson, A. S.; Kalska, B.; Häggström, L.; Thomas, J. O. *Solid State Ionics* **2000**, *130*, 41–52.
(11) Needham, S. A.; Calka, A.; Wang, G. X.; Mosbah, A.; Liu, H. K. *Electrochem. Commun.* **2006**, *8*, 434–438.
(12) Ravet, N.; Chouinard, Y.; Magnan, J. F.; Besner, S.; Gauthier, M.; Armand, M. *J. Power Sources* **2001**, *97−98*, 503–507.
(13) Chen, Z. H.; Dahn, J. R. *J. Electrochem. Soc.* **2002**, *149*, A1184–A1189.
(14) Yang, S. F.; Zavalij, P. Y.; Whittingham, M. S. *Electrochem. Commun.* **2001**, *3*, 505–508.
(15) Huang, H.; Yin, S.-C.; Nazar, L. F. *Electrochem. Solid-State Lett.* **2001**, *4*, A170.
(16) Andersson, A. S.; Thomas, J. O. *J. Power Sources* **2001**, *97−98*, 498–502.
(17) Yamada, A.; Koizumi, H.; Sonoyama, N.; Kanno, R. *Electrochem. Solid-State Lett.* **2005**, *8*, A409−A413.
(18) Meethong, N.; Huang, H. Y. S.; Carter, W. C.; Chiang, Y. M. *Electrochem. Solid-State Lett.* **2007**, *10*, A134−A138.
(19) Chen, G. Y.; Song, X. Y.; Richardson, T. J. *Electrochem. Solid-State Lett.* **2006**, *9*, A295–A298.
(20) Laffont, L.; Delacourt, C.; Gibot, P.; Wu, M. Y.; Kooyman, P.; Masquelier, C.; Tarascon, J. M. *Chem. Mater.* **2006**, *18*, 5520–5529.

10.1021/cm801995p CCC: $40.75
Published on Web 10/25/2008

Morgan et al. and Islam et al.,[21,22] but invalidating the shrinking-core model.

Recently, we focused our interest on the optimization of carbon-coated $LiFePO_4$ samples (C-$LiFePO_4$) synthesized by mechanochemical activated mixture of phosphate precursors with cellulose to get a high reversible capacity. a general characterization of the starting materials and of the deintercalated ones was performed in order to try to understand the involved processes.[23−25] These carbon-coated $LiFePO_4$ samples were shown to be nanosized materials (around 100 nm in diameter) that can be used at very high rate in lithium-ion batteries. X-ray diffraction and high-resolution transmission electron microscopy showed the existence at any state of charge (or discharge) of a mixture of fully intercalated and fully deintercalated primary particles.[25] According to these results, we proposed the Domino−Cascade model to describe lithium deintercalation from $LiFePO_4$. There is concentration of structural constraints and charge carriers at the boundary between $FePO_4$ and $LiFePO_4$ domains leading locally to an ionic and electronic conductivity considerably higher than in the two end-member phases. Therefore, the growth of one phase at the expense of the other one is considerably faster than the nucleation of a new domain. The intercalation (deintercalation) mechanism results in fact from a very fast displacement of the reaction front along the *a*-axis without any energy barrier.

X-ray photoelectron spectroscopy (XPS) allows us to access the local environment of atoms and their oxidation states, and thus in this paper it will allow us to follow redox processes occurring in C-$LiFePO_4$ during the lithium deintercalation/intercalation reaction. Because of its surface sensitivity (analysis depth around 5 nm), it will provide additional information about the two-phase reaction. Because our C-$LiFePO_4$ samples display an average primary particle size around 100 nm, XPS will allow us to access the mechanisms at the very surface of the particles, and thus will bring an additional element in the argumentation between the models considering migration of a reaction front along the *a*-axis[19,20,25] vs. the shrinking-core model, still considered in the litterature by some authors to describe the electrochemical process in $LiFePO_4$.[26,27]

In this paper, we will also follow changes occurring at the positive electrode/electrolyte interface. Indeed, as these samples are nanosized materials, they may activate electrolyte degradation at their surface during the electrochemical processes. The knowledge of these surface reactions is essential as they can have an impact on the Li//C-$LiFePO_4$ lithium-ion battery cycle life.

2. Experimental Section

The carbon-coated $LiFePO_4$ sample was synthesized by a preliminary mechano-chemical activation of the precursors and then a thermal treatment of this mixture at 575 °C. The reactants, "iron phosphate", whose synthesis is performed through precipitation of iron sulfate $FeSO_4 \cdot 7H_2O$ in a sodium phosphate solution (Na_3PO_4), and lithium phosphate (Aldrich), were mixed such as Li/Fe ≈ 1.05. That Li/Fe ratio was chosen in agreement with previous studies performed by some of us that showed formation of $Fe_2P_2O_7$ as impurity in $LiFePO_4$ samples for nominal Li/Fe ratios equal to 1. Cellulose (Aldrich) was also initially added (10 wt %) to these precursors. The so obtained mixture was ball-milled (∼50 g) four times 1 h 30 min. in a planetary mill (Fritsch "Pulverisette 4") using tungsten carbide vessels (250 mL) and 14 agate balls (diameter 10 mm). Between each run, powder was removed from walls under a controlled atmosphere. The resulting mixture was finally thermal-treated at 575 °C in a tubular furnace under argon flow.

Chemical analyses gave a Li/Fe ratio of ∼1.06−1.08 and P/Fe ≈ 1.01−1.04, and Mössbauer spectroscopy revealed ∼5−6 at % of Fe^{3+} ions. Nevertheless, from an X-ray diffraction point of view, the obtained material is a pure olivine-type phase, well-ordered with an ideal cation distribution within the structure. Mössbauer spectroscopy and magnetic measurements also excluded the presence of a crystalline ferro- or ferrimagnetic impurity rich in Fe^{3+} ions; but the presence of either an amorphous impurity rich in Fe^{3+} ions or surface defects can not be excluded.

"Li_xFePO_4" materials were obtained through electrochemical lithium deintercalation (intercalation) from cast electrodes. These cast electrodes were prepared from a 500 mg mixture of 80 wt % carbon-coated $LiFePO_4$ active material with 10 wt % carbon conductive additive (Super P, MMM Carbon) and 10 wt % poly(vinylidene fluoride) (PVDF) binder (Solef 6020, Solvay), as well as with 0.8 mg of *N*-methyl pyrrolidone. This mixture was then cast on an aluminum foil and dried one night at 55 °C. Pellets of 10 mm diameter were finally punched, pressed at 10 T cm^{-2} and dried for 48 h at 80 °C under a vacuum. Considering their surface and thickness, a mass smaller than 2 mg for the active material was cast on each electrode, leading then to an average error of approximately ±5% on the reversible capacity. These electrodes were then charged up (or, charged and discharged down) to a given lithium composition in laboratory lithium cells also containing a lithium foil as negative electrode, two separators and a polypropylene foil wetted by a liquid electrolyte (1 M $LiPF_6$ in a mixture of propylene carbonate (PC)−ethylene carbonate (EC)−dimethyl carbonate (DMC) (1.1.3)). These lithium cells were assembled in a dry box under argon. Electrochemical tests were carried out with a Biologic VMP1 apparatus in galvanostatic mode at a constant *C*/20 rate in the potential window [2−4.5] V. The *C*/*n* rate is defined such as the theoretical capacity is obtained during a charge in *n* hours. It means thus in the present study that a charge in *n* hours is necessary at a *C*/*n* rate for an exchange of one electron (or deintercalation of one lithium from $LiFePO_4$).

After cycling, "Li_xFePO_4" positive electrodes (i.e., XPS samples) were recovered in dry inert atmosphere, washed with DMC to remove the $LiPF_6$ salt and then dried under a vacuum. The XPS sample-holder was prepared in a nitrogen dry box directly connected through a transfer chamber to the XPS spectrometer, which prevents any exposure of the samples to moisture/air. XPS analyses were carried out with a Kratos Axis Ultra spectrometer using a focused monochromatized Al Kα radiation ($h\nu$ = 1486.6 eV). The

(21) Morgan, D.; Van der Ven, A.; Ceder, G. *Electrochem. Solid-State Lett.* **2004**, *7*, A30–A32.
(22) Islam, M. S.; Driscoll, D. J. J.; Fisher, C. A.; Slater, P. R. *Chem. Mater.* **2005**, *17*, 5085–5092.
(23) Maccario, M.; Croguennec, L.; Wattiaux, A.; Suard, E.; Le Cras, F.; Delmas, C. *Solid State Ionics* **2008**, doi.10.1016/j.ssi.2008.07.004, in press.
(24) Maccario, M. PhD thesis. University of Bordeaux 1, Pessac, France, 2007.
(25) Delmas, C.; Maccario, M.; Croguennec, L.; Le Cras, F.; Weill, F. *Nat. Mater.* **2008**, in press.
(26) Meethong, N.; Shadow Huang, H.-Y.; Speakman, S. A.; Carter, W. C.; Chiang, Y.-M. *Adv. Funct. Mater.* **2007**, *17*, 1115–1123.
(27) Srinivasan, V.; Newman, J. *J. Electrochem. Soc.* **2004**, *151*, A1517–A1529.

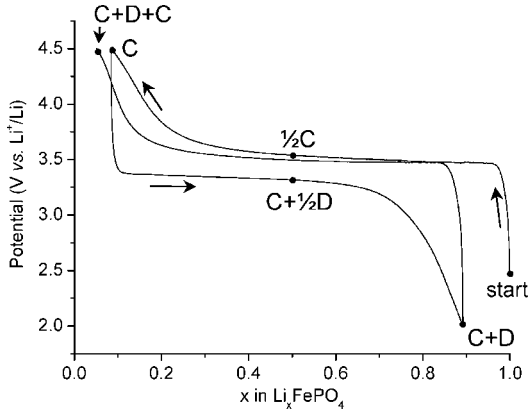

Figure 1. Cycling curve obtained at C/20 in the [2−4.5] V potential window (vs Li^+/Li) for a Li//C-$LiFePO_4$ cell. Compositions studied ex situ by XPS are highlighted by points.

spectrometer was calibrated using the photoemission line Ag $3d_{5/2}$ (binding energy 368.3 eV). Spectra were recorded with 20 eV constant pass energy. The analyzed area of the samples was 300 × 700 μm^2, charge neutralization was used and the pressure in the analysis chamber was ca. 5×10^{-7} Pa. Short-time spectra were recorded before and after each experiment and compared, to check the nondegradation of the samples in the X-Ray beam. The binding energy (BE) scale was calibrated from C 1s peaks of PVDF used in the electrodes (CF_2 and CH_2 at 290.9 and 286.4 eV, respectively). Peak positions and areas were obtained by a weighted least-squares fitting of model curves (70% Gaussian, 30% Lorentzian) to the experimental data. Quantification was performed on the basis of Scofield's relative sensitivity factors.

3. Results and Discussion

Figure 1 shows the electrochemical curve of a Li//C-$LiFePO_4$ cell. The points (•) show the various "Li_xFePO_4" average compositions synthesized and studied ex situ by XPS. The XPS spectra were at first carefully analyzed for the carbon-coated $LiFePO_4$ pristine material, either as powder or as cast electrode. Then, its changes upon lithium deintercalation/intercalation were followed and analyzed.

3.1. Fresh C-$LiFePO_4$ Material (Powder Pristine Material and Cast Electrode). Fe 2p, Fe 3s, P 2p, O 1s, and C 1s spectra obtained for the pristine powder material $LiFePO_4$ and the freshly prepared cast electrode are compared in Figure 2 a-e. Note that the Li 1s peak (∼55 eV) is not shown here; in fact it is totally obscured by the Fe 3p peak, because its relative sensitivity factor is about 30 times smaller than that of Fe 3p.

As shown in Figure 2a, Fe 2p spectra are split in two parts due to spin−orbit coupling, namely Fe $2p_{3/2}$ and Fe $2p_{1/2}$, with an intensity ratio of about 2/1. Each part consists of a main peak and a "shake-up" satellite.[28] $LiFePO_4$ shows a Fe $2p_{3/2}$ main peak at 710 eV with a satellite peak at ∼ 715 eV (∼724 and ∼729 eV for Fe $2p_{1/2}$, respectively). The spectra of the powder pristine material and the freshly prepared cast electrode are in good agreement with Fe^{2+} ions in an oxygen environment. It is interesting to highlight that the fine structure of the Fe $2p_{3/2}$ main peak (at 709.5 and 710.5 eV) in Figure 2a cannot be explained by the presence of Fe^{3+} ions. It would rather be explained by a multiplet effect.[28] First, because the XPS signature of Fe^{3+} is very different, as it will be observed in Figure 3 for "Li_xFePO_4" deintercalated samples. Second, because the $\Delta E = 5.7$ eV splitting observed in the Fe 3s spectrum (Figure 2b) is also characteristic of Fe^{2+}.[28] It results from the exchange interaction of Fe 3s and 3d electrons, leading to an energy difference between two photoemission final states with the 3s spin parallel or antiparallel to the 3d spin. The magnitude of the Fe 3s splitting is roughly proportional to $(2S + 1)G^2(3s,3d)/5$, where S is the value of the local 3d spin and $G^2(3s,3d)$ is the Slater exchange integral between the 3s and the 3d electrons.[29] As a result, the Fe 3s splitting is dependent on the number of 3d electrons. a 5.7 eV splitting is characteristic of Fe^{2+}, whereas an ∼ 6.5 eV value is expected for Fe^{3+} ions. However, XPS spectra do not allow us to exclude the presence of a small amount of Fe^{3+} at the surface of the sample, because 5−6 at % Fe^{3+} was observed by Mössbauer spectroscopy.[24]

The P 2p spectrum shown in Figure 2c is also split in two components $2p_{3/2}$ and $2p_{1/2}$ due to spin−orbit coupling (133.4 and 134.3 eV, respectively). The observation of only one P 2p doublet at this binding energy reveals the presence of only one environment for phosphorus, in good agreement with a $(PO_4)^{3-}$ phosphate group. Furthermore, the presence of iron phosphide (Fe_2P or Fe_3P) as suggested by some other studies[30,31] can be excluded here because the characteristic P 2p peak of a phosphide at about 129.5 eV is not observed.[32,33] The P 2p spectra are similar for the two samples (powder and cast electrode).

Figure 2d shows O 1s core peaks of the powder pristine material and freshly prepared cast electrode. Both spectra display a narrow peak at 531.4 eV which is attributed to oxygen atoms of $(PO_4)^{3-}$ phosphate groups. The spectrum of the powder pristine material displays a weak component at 533.2 eV, which can be assigned to contaminating species adsorbed at the surface. The spectrum of the cast electrode shows additional contaminating species ensuing from electrode manufacturing.

Figure 2e shows C 1s core peaks of the pristine powder and the cast electrode. The spectrum of the pristine material displays an asymmetric peak at 284.6 eV, which is assigned to the carbon coating of C-$LiFePO_4$ obtained by cellulose decomposition at 575 °C. This asymmetric shape is similar to that observed for graphite, but the fwhm is much greater here (1.2 eV instead of 0.6 eV). XPS quantification reveals the presence of 43 at % carbon vs 57 at % $LiFePO_4$ at the surface of the particles (whereas it is only 4.6 at % on average in the sample), showing the efficiency of the carbon coating.

(28) Hüfner, S, *Photoelectron Spectroscopy: Principles and Applications*; Springer-Verlag: Weinheim, Germany, 1995.
(29) Saitoh, T.; Bocquet, A. E.; Mizokawa, T.; Namatame, H.; Fujimori, A.; Abbate, M.; Takeda, Y.; Takano, M. *Phys. Rev. B* **1995**, *51*, 13942.
(30) Ait Salah, A.; Mauger, A.; Julien, C. M.; Gendron, F. *Mater. Sci. Eng., B* **2006**, *129*, 232–244.
(31) Herle, P. S.; Ellis, B.; Coombs, N.; Nazar, L. F. *Nat. Mater.* **2004**, *3*, 147–152.
(32) Wagner, C. D.; Naumkin, A. V.; Kraut-Vass, A.; Allison, J. W.; Powell, C. J.; Rumble, J. R. J. NIST Standard Reference Database 20, version 3.4 (Web version); National Institute of Standards and Technology: Gaithersburg, MD, 2006.
(33) Myers, C. E.; Franzen, H. F.; eregg, J. W. *Inorg. Chem.* **1985**, *24*, 1822–1824.

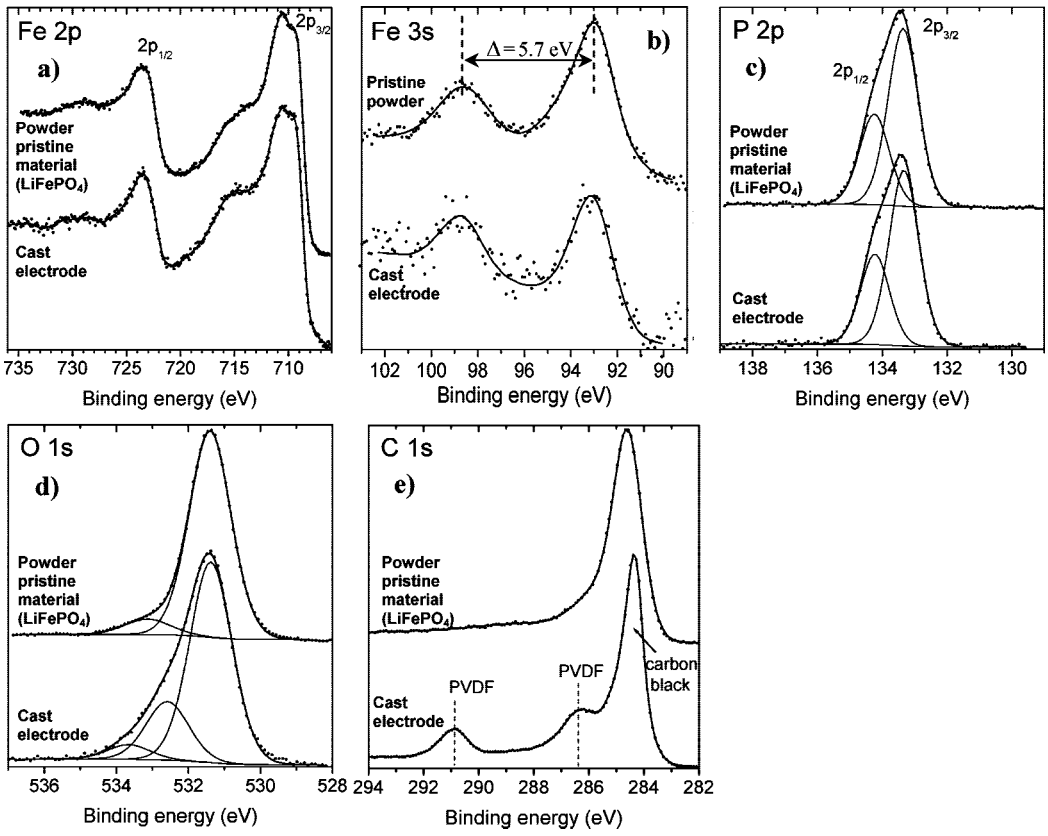

Figure 2. Fe 2p, Fe 3s, P 2p, O 1s, and C 1s XPS core peaks of the powder pristine material $LiFePO_4$ and of the cast electrode freshly made from this powder.

The C 1s spectrum of the cast electrode is completely modified by the use of additives for the electrode elaboration. Indeed, two new peaks are observed at 291.9 and 286.4 eV, which can be attributed to the PVDF $(CH_2-CF_2)_n$ binder. The main peak at 284.3 eV is associated to carbon black and totally obscures the peak of the carbonaceous coating of C-$LiFePO_4$. This is due to the great specific surface area of carbon black particles and to the covering effect of PVDF binder at the surface of C-$LiFePO_4$ particles.

3.2. Cycled C-$LiFePO_4$ Material. *3.2.1. Intercalation/Deintercalation Reaction.* Figure 3 shows the evolution of Fe 2p and Fe 3p XPS spectra for "Li_xFePO_4" cast electrodes recovered at different states of charge or discharge of Li||$LiFePO_4$ cells cycled at *C*/20 in the [2−4.5] V potential window (vs Li^+/Li).

Both Fe $2p_{3/2}$ and $2p_{1/2}$ components show the same changes. During the first charge, the Fe $2p_{3/2}$ spectrum displays a gradual decrease of the main peak at 710 eV (characteristic of Fe^{2+}), and a gradual enhancement of a new peak at 711−712 eV (characteristic of Fe^{3+}), showing the disappearance of the lithium-rich phase $Li_{1-\varepsilon}FePO_4$ parallel to the appearance of the new lithium-deficient phase $Li_{\varepsilon'}FePO_4$. The spectrum characteristic of Fe^{3+} also shows a complex profile, and thus it is not possible to give quantitative values for the Fe^{3+}/Fe^{2+} ratio during charge. Note that a small Fe^{2+} shoulder still remains in the Fe $2p_{3/2}$ spectrum at the end of the charge (*C*), as expected due to an average composition of $Li_{\sim 0.08}FePO_4$ for the electrode.

During the following discharge, the opposite process is observed, with a gradual decrease of the Fe^{3+} peak and a gradual enhancement of the Fe^{2+} peak. The spectrum obtained after 1 charge + $^1/_2$ discharge ($C + {}^1/_2D$) is very similar in shape, position, and intensity to that obtained after $^1/_2$ charge ($^1/_2C$). In the same way, the spectrum obtained after 1 cycle ($C + D$) is very similar to that of the freshly prepared electrode. The spectra obtained after the first and the second charges (C and $C + D + C$) are also very similar (the small Fe^{2+} shoulder is observed for the two, in good agreement with average lithium compositions of ∼0.08 and ∼0.05, respectively). This study shows thus the good reversibility of the Fe^{3+}/Fe^{2+} redox process upon charge/discharge cycles.

Fe 3p spectra (Figure 3b) show the same evolution. The 55 eV peak (characteristic of Fe^{2+}) is gradually replaced by a peak at 57 eV (characteristic of Fe^{3+}) upon charge, and the opposite process is observed upon discharge. Fe^{3+} is in large majority in the sample at the end of charge (C). Note that Fe 3p and Fe 2p provide complementary information, because they are associated with different analysis depths. Indeed, the kinetic energy of the photoelectrons coming into the analyzer is around 770 eV for Fe 2p and 1430 eV for Fe 3p, resulting in a photoelectron escape depth about 1.5 times greater for Fe 3p than for Fe 2p. Therefore, Fe 3p spectra are slightly more representative of the bulk material than Fe 2p. It should be also noted that the Li 1s core peak is totally obscured by Fe 3p, as said before. However, it does not hinder the analysis of Fe 3p, first because of its very weak relative sensitivity factor, and second because only weak amounts of lithiated species are formed at the surface upon cycling, as we will see hereafter.

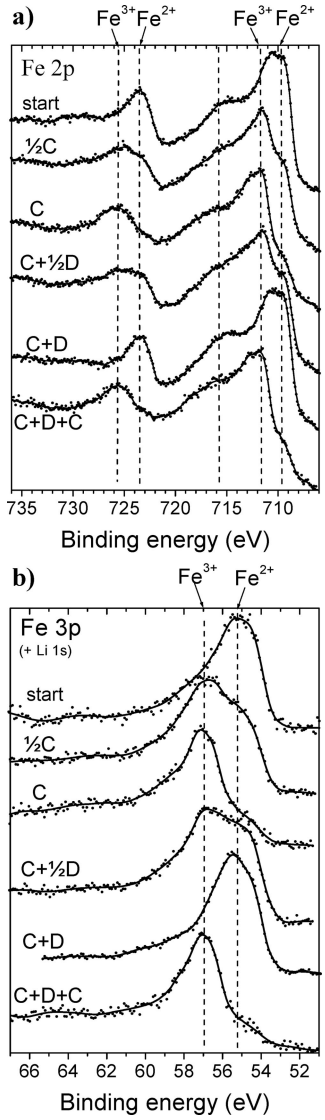

Figure 3. Fe 2p and Fe 3p XPS core peaks obtained for "Li_xFePO_4" cast electrodes recovered at different states of charge or discharge of Li}$LiFePO_4$ cells cycled at C/20 in the [2−4.5] V potential window (vs Li^+/Li).

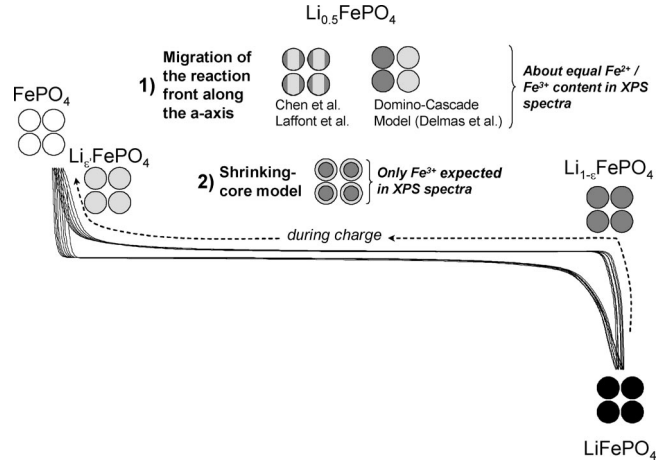

Figure 4. Scheme to describe the expected XPS spectra according to either. (1) Models considering migration of the reaction front along the *a*-axis,[19,20,25] or (2) the shrinking-core model.[1,26,27]

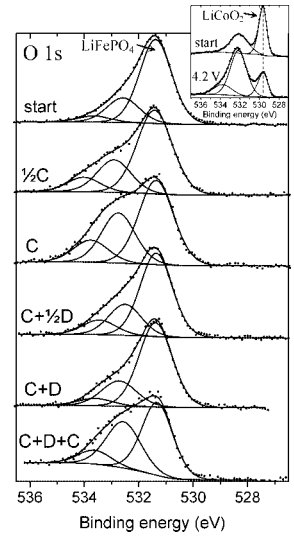

Figure 5. O 1s XPS core peaks of "Li_xFePO_4" cast electrodes recovered at different states of charge or discharge of Li }$LiFePO_4$ cells cycled at C/20 in the [2−4.5] V potential window (vs Li^+/Li). The right corner inset corresponds to the results obtained with a LiCoO2 electrode charged at 4.2 V (vs Li^+/Li) in similar conditions, for comparison.

As a summary, XPS Fe 2p and 3p core peaks allow to reach the same conclusions as Mössbauer spectroscopy[24] for this sample, i.e., a continuous evolution of the Fe^{3+}/Fe^{2+} ratio upon charge and discharge, in good agreement with the change in the average lithium content of the electrodes (Note that our Mössbauer measurements upon cycling are not presented here because they were very similar to those reported by Thomas and co-workers [10]). Because XPS provides an analysis of the surface and Mössbauer spectroscopy an analysis of the bulk, there is no apparent difference between the bulk and the surface of the particles during the redox mechanisms occurring upon lithium deintercalation/intercalation in "Li_xFePO_4". Figure 4 gives a schematic overview of the $LiFePO_4/FePO_4$ domains distribution during lithium deintercalation from $LiFePO_4$, according to the various models proposed in literature. If the shrinking-core model was involved during the reaction, a very large Fe^{3+}/Fe^{2+} ratio would be observed at half-charge at the surface of the particles in XPS spectra. The results obtained show clearly that this mechanism does not occur and that whatever the state of charge (respectively discharge) there is a continuous increase (respectively decrease) of the Fe^{3+}/Fe^{2+} ratio, in good agreement with the average lithium composition of the Li_xFePO_4 electrode material. On the contrary, these XPS results are consistent with the results recently obtained by Chen et al. and Laffont et al.,[19,20] i.e. with the formation of $Li_{1-\varepsilon}FePO_4$ and $Li_{\epsilon'}FePO_4$ domains in crystallites of Li_xFePO_4 composition, and also with the Domino-Cascade model reported more recently by some of us for $LiFePO_4$ nanoparticles,[25] i.e. with the formation of single-phase ($Li_{1-\varepsilon}FePO_4$ or $Li_{\varepsilon'}FePO_4$) crystallites at any state of charge or discharge with the right ratio to accommodate the average Li_xFePO_4 composition for the sample.

3.2.2. Electrode/Electrolyte Interface. Concerning the electrode/electrolyte interface, other XPS core peaks provide additional information. Figure 5 shows O 1s spectra of the same samples. We can first notice that the characteristic peak of $LiFePO_4$ at 531.4 eV still remains the main peak of the O 1s spectrum during the whole electrochemical cycling.

One can also notice the increase of two O 1s components at ~ 532.5−533 eV and ~533.5−534 eV upon charge, showing the deposition of a small amount of oxygenated species ensuing from electrolyte degradation. These species may be organic or inorganic, as it is commonly observed at the surface of graphite electrodes.[34] Unfortunately, the identification of organic species in our case is difficult because C 1s spectra are largely dominated by the PVDF binder and the carbon additive, so that no evolution of the C 1s spectra can be observed from the fresh electrode to the end of the cycle (for this reason, C 1s spectra have not been shown). The second observation from Figure 5 is that the amount of deposited species at the surface decreases upon discharge, and increases again during the second charge, showing some dynamic behavior of the electrode/electrolyte interface. This was already observed at the surface of both electrodes of the $LiCoO_2$/graphite system[35] and at the surface of noncarbonaceous negative electrodes.[36]

However, the most important point here is that the characteristic peak of $LiFePO_4$ at 531.4 eV still remains the main peak of the O 1s spectrum during cycling. This behavior is rather different from that of $LiCoO_2$ in the same electrochemical conditions. To highlight this difference of behavior, we have reported the O 1s spectra of a $LiCoO_2$ electrode before and after charge at 4.2 V (vs Li^+/Li) in similar cycling conditions in the top right corner inset of Figure 5. In this inset, we can see that a rather large number of oxygenated species are deposited at the surface of the $LiCoO_2$ electrode upon charge, leading to a significant decrease in the O 1s component of $LiCoO_2$ due to the analysis depth. This behavior is very different for $LiFePO_4$. This is a noteworthy result, because the potential at the end of charge is very high (4.5 V vs Li^+/Li) and the C-$LiFePO_4$ particles are nanosized. Therefore, one would have expected an enhanced reactivity of the surface of the particles toward the electrolyte upon charge, which is not observed here. This result shows that only a weak amount of oxygenated species are deposited at the surface of the electrode, and explains why the Fe 3p spectrum shown in Figure 3 was not disturbed by the Li 1s spectrum at the same binding energy, because the amount of lithiated species deposited at the electrode/electrolyte interface is rather low. The surface of the C-$LiFePO_4$ particles is thus not very reactive toward the electrolyte.

Figure 6 shows P 2p spectra of the same samples. Here again the $2p_{3/2}$-$2p_{1/2}$ doublet at 133.4−134.3 eV assigned to the active material $LiFePO_4$ still remains the main component of the spectrum upon the electrochemical cycling. However, a slight broadening of the spectrum can be noticed, connected with a slight increase of the measured amount of phosphorus. This can be explained by the appearance of new phosphorus-containing species, with appearance of a new P 2p doublet with the $2p_{3/2}$ component at 134.0 eV. This binding energy value is commonly observed by XPS at electrode/electrolyte

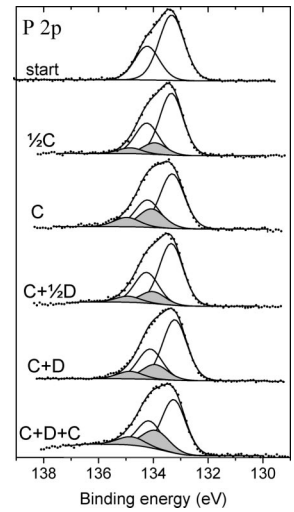

Figure 6. P 2p XPS core peaks of "Li_xFePO_4" cast electrodes recovered at different states of charge or discharge of Li }$LiFePO_4$ cells cycled at C/20 in the [2−4.5] V potential window (vs Li^+/Li).

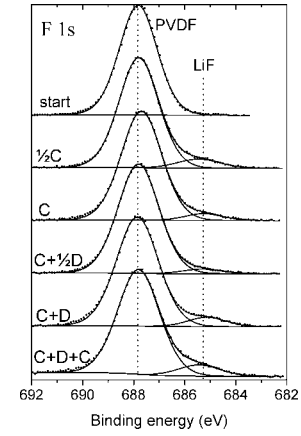

Figure 7. F 1s XPS core peaks of "Li_xFePO_4" cast electrodes recovered at different states of charge or discharge of Li }$LiFePO_4$ cells cycled at *C*/20 in the [2 −4.5] V potential window (vs Li^+/Li).

interfaces of Li-ion batteries.[35,37] It corresponds to a small amount of phosphate species coming from the degradation of the salt $LiPF_6$. Several mechanisms have been proposed to explain the formation of these phosphate species,[38] particularly by reaction of $LiPF_6$ with the traces of water in the electrolyte. No particular reversible mechanism can be evidenced upon charge and discharge, as it was observed for the O 1s spectra.

Figure 7 shows the corresponding F 1s spectra. Very few changes are observed upon cycling. The spectra consist of a main peak assigned to the PVDF binder and of a small peak attributed to lithium fluoride LiF, also coming from degradation reactions of the salt $LiPF_6$. The amount of LiF deposited at the surface of the electrodes is quite low (2−5%), as compared to $LiCoO_2$ in similar conditions (up to 18%).[39] As for the P 2p peak, no particular reversible mechanism

(34) Aurbach, D. *J. Power Sources* **2000**, *89*, 206–218.
(35) Leroy, S.; Blanchard, F.; Dedryvère, R.; Martinez, H.; Carré, B.; Lemordant, D.; Gonbeau, D. *Surf. Interface Anal.* **2005**, *37*, 773–781.
(36) Stjerndahl, M.; Bryngelsson, H.; Gustafsson, T.; Vaughey, J. T.; Thackeray, M. M.; Edström, K. *Electrochim. Acta* **2007**, *52*, 4947–4955.
(37) Andersson, A. M.; Abraham, D. P.; Haasch, R.; MacLaren, S.; Liu, J.; Amine, K. *J. Electrochem. Soc.* **2002**, *149*, A1358–A1369.
(38) Vetter, J.; Novak, P.; Wagner, M. R.; Veit, C.; Moller, K. C.; Besenhard, J. O.; Winter, M.; Wohlfahrt Mehrens, M.; Vogler, C.; Hammouche, A. *J. Power Sources* **2005**, *147*, 269–281.
(39) Dedryvère, R.; Martinez, H.; Leroy, S.; Lemordant, D.; Bonhomme, F.; Biensan, P.; Gonbeau, D *J. Power Sources* **2007**, *174*, 462–468.

can be evidenced upon charge and discharge. The slight increase of the amount of LiF may rather be due to time-dependent aging of the electrolyte.

As a summary, the changes observed for P 2p and F 1s spectra upon electrochemical cycling are different from those observed for O 1s spectra. Indeed phosphate species and LiF are formed during the first charge and kept upon discharge whereas along electrochemical cycle oxygenated species are partially formed/dissolved, meaning that the particular O 1s spectrum shape upon charge can be explained by the appearance of organic species resulting from the degradation of solvents of the electrolyte. However, the amount of oxygenated degradation species is very low as compared to other positive electrode materials such as $LiCoO_2$. Our results are slightly different from those obtained by Herstedt et al.[40,41] for the characterization of the interface formed on carbon-treated $LiFePO_4$ particles after electrochemical cycling. They observed no degradation products from solvent reactions at the surface of the electrodes, but the electrode/electrolyte interface was dominated by salt degradation reactions, resulting in a surface layer thick enough to make iron not visible by XPS, which is not our case here. Note that their experimental conditions were very different from ours. their XPS samples were obtained after three electrochemical cycles in a narrower potential window [2.7−4.1] V vs Li^+/Li at *C*/20 rate at 23 or 40 °C followed by a storage for one week, and without washing the electrodes by the solvent. However, the main conclusion of these authors was that the surface chemistry of $LiFePO_4$ is different from that of other positive electrode materials, because it is rather weakly reactive toward solvents. We draw the same conclusions for nanosized C-$LiFePO_4$.

Note that we obtained similar results for C-$LiFePO_4$ materials prepared according to the same synthesis method but at a higher temperature (800 °C instead of 575 °C here). For all the composites, XPS analyses confirmed the gradual oxidation of Fe^{2+} into Fe^{3+} upon charge and the gradual reduction of Fe^{3+} into Fe^{2+} upon discharge, showing that the redox processes do not match the shrinking-core model. Despite a slightly smaller specific surface area, the amount of degradation products formed at the surface of the electrode was not significantly different from that observed for the samples synthesized at 575 °C. Despite the nanosize of these materials, their great specific surface area does not result in the formation of a thick passivation layer. Therefore, the amount of lithium lost by the formation of this interface does not seem to be a drastic drawback for the use of this kind of electrodes in lithium-ion batteries as shown by promising long time cycling performance obtained at 25 or 40 °C.[42]

4. Conclusion

In this work, we have investigated the redox processes undergone by nanosized carbon-coated $LiFePO_4$ samples used as positive electrode material in lithium-ion batteries. XPS analyses revealed a continuous evolution of the Fe^{3+}/Fe^{2+} ratio at the surface of the particles upon charge and discharge, in good agreement with the change in the average lithium content of the particles driven by the electrochemical reaction, and thus rejecting the assumption that a $FePO_4$/$LiFePO_4$ interface migrates from the surface to the core of each particle upon charge, with the reverse mechanism upon discharge. This confirms the models considering migration of a reaction front along the *a*-axis inside the particles to the detriment of the "shrinking-core" model. Moreover, XPS analyses showed the formation of a much thinner surface film at the surface of the C-$LiFePO_4$ particles than for other positive electrode materials such as $LiCoO_2$, despite the nanometric size of the particles. This suggests that electrode/electrolyte interface phenomena may not limit performances of lithium-ion batteries using C-$LiFePO_4$ particles as positive electrode material.

Acknowledgment. The authors thank Région Aquitaine (CPER Véhicule électrique 21 − 13), Ademe (Convention 03 66 C0072), and CEA for financial support.

CM801995P

(40) Herstedt, M.; Stjerndahl, M.; Nyten, A.; Gustafsson, T.; Rensmo, H.; Siegbahn, H.; Ravet, N.; Armand, M.; Thomas, J. O.; Edstrom, K. *Electrochem. Solid-State Lett.* **2003**, *6*, A202–A206.

(41) Edström, K.; Gustafsson, T.; Thomas, J. O. *Electrochim. Acta* **2004**, *50*, 397–403.

(42) Maccario, M.; Croguennec, L.; Le Cras, F.; Delmas, C. *; J. Power Sources* **2008**, *183*, 411–417.